

Ultra-broadband High Coupling Efficiency Fiber-to-Waveguide Coupler Using $\text{Si}_3\text{N}_4/\text{SiO}_2$ Waveguides On Silicon

Tiecheng Zhu,¹ Yiwen Hu,¹ Pradip Gatkine,² Sylvain Veilleux,² Joss Bland-Hawthorn,³ Mario Dagenais,¹ *Fellow, IEEE*

¹*Department of Electrical and Computer Engineering, University of Maryland, College Park, MD 20742, USA*

²*Department of Astronomy and Joint Space-Science Institute, University of Maryland, College Park, MD 20742, USA*

³*Sydney Institute for Astronomy and Sydney Astrophotonic Instrumentation Labs, School of Physics, The University of Sydney, NSW 2006, Australia*

Abstract: An easy-to-fabricate but very efficient fiber-to-waveguide coupler is theoretically analyzed and experimentally demonstrated. In this design, light from a single-mode fiber can be butt-coupled into a single-mode high-index-contrast $\text{Si}_3\text{N}_4/\text{SiO}_2$ waveguide with a measured coupling efficiency of 96 % at the wavelength of 1550 nm, and > 90 % in the spectral range from 1450 nm to 1650 nm. Large horizontal and vertical alignment tolerances of 3.8 μm and 3.6 μm respectively are obtained between the fiber and the waveguide coupler. All these experimental results agree well with simulations. The waveguide coupler also features ease of end-facet cleaving, and can be used in ultra-broadband high coupling efficiency applications.

Index Terms: Waveguides, Photonic integrated circuits, Integrated optics devices.

1. Introduction

$\text{Si}_3\text{N}_4/\text{SiO}_2$ waveguides on silicon find applications in communication, signal processing, optical sensors, narrow-band filters, photonic band gap engineering, on-chip optical frequency comb generation, short pulse generation and photonic integrated circuits for optical interconnects [1] [2] [3] [4] [5] [6] [7]. Compared with Silicon-on-Insulator (SOI) technology which absorbs light below the wavelength of 1.1 μm , $\text{Si}_3\text{N}_4/\text{SiO}_2$ waveguide has the advantage of a larger transparent spectrum and ultra-low propagation loss [8] [9]. The index contrast between Si_3N_4 and SiO_2 , although not as high as that in the SOI waveguides, is still large enough to realize reasonably confined waveguides for integration. As for any integration platform, one of the key issues is how to couple light efficiently from an optical fiber into a planar waveguide.

Generally speaking, there are three major approaches for achieving a high coupling efficiency between an optical fiber and a $\text{Si}_3\text{N}_4/\text{SiO}_2$ waveguide. The first approach utilizes the grating coupler (GC), where the light is launched from an optical fiber into a GC at an oblique angle [10]. A large number of studies have been focused on improving the coupling efficiencies by using a GC [11] [12] [13]. One drawback of the GCs is that these devices are not usually broadband, because of requirements related to phase matching, which can only be met near the central wavelength. Moreover, since a GC typically couples the light from a single-mode optical fiber to a multi-mode waveguide, a subsequent mode-converter is necessary for bringing the light back to a single-mode confined waveguide, and this introduces extra loss.

The second popular approach to achieving a high coupling efficiency between an optical fiber and a $\text{Si}_3\text{N}_4/\text{SiO}_2$ waveguide is to use a taper at both ends of the waveguide [14] [15]. The taper-based couplers are inherently more broadband than the GC-based couplers, but in most cases, it requires a precise end-facet cleaving process to achieve a high coupling efficiency. Finally, the third approach of coupling relies on the concept of evanescent-field coupling, where efficient coupling is realized between an overlap region between a single-sided conical tapered fiber and a tapered $\text{Si}_3\text{N}_4/\text{SiO}_2$ waveguide [16]. Although the results are promising, it is hard to apply this technique for coupling to multiple devices or for large scale integration.

In this paper, we demonstrate a fiber-to-waveguide coupler implemented on the $\text{Si}_3\text{N}_4/\text{SiO}_2$ waveguides on silicon substrate using Si_3N_4 as the core material and SiO_2 as the cladding material. This coupler features ultra high coupling efficiency (98 % in theory and 96 % in experiment) for a ultra-broadband transmission spectrum, ease of cleaving and large alignment tolerances. The approach introduced here is also applicable for multi-device operations. In Section 2, we first present a theoretical analysis of the coupling efficiencies for different varying parameters (i.e. thickness of layers, waveguide width, etc). Then, in Section 3 the couplers are fabricated and the coupling efficiencies and the alignment tolerances are characterized experimentally. In Section 4, we discuss further improvements and potential applications suitable for the waveguide coupler. Finally, in Section 5, we conclude and briefly discuss future work.

2. Design and Modeling

2.1. Waveguide Coupler Design

Fig. 1 shows the waveguide coupling geometry. The waveguide coupler, which has Si_3N_4 as the core layer and SiO_2 as both the top and bottom cladding layers, is implemented on the $\text{Si}_3\text{N}_4/\text{SiO}_2$ waveguides on silicon substrate to obtain a larger spectral transparency window. Compared with the SOI platform which absorbs light below $1.1 \mu\text{m}$, a $\text{Si}_3\text{N}_4/\text{SiO}_2$ waveguide is transparent for both the visible and the near-infrared spectra. Having such a large spectral operation range is of particular interest in many areas, such as sensors and astronomy applications [17] [18].

As shown in Fig. 1, the whole waveguide coupler is composed of three parts. Part I is a loosely-confined straight waveguide whose mode profile is designed to optimize the coupling with the fiber. As will be shown later, the geometry of the Part I waveguide is optimized to realize a ultra-broadband coupling efficiency over a wide spectrum. Another important advantage of the Part I waveguide is that it allows ease of end-facet cleaving. The position of the cleaving is not important for realizing high coupling efficiency, as long as the cleaving takes place within Part I of the waveguide. The waveguide coupler in this paper is designed to butt-couple with the optical fiber. Compared with other coupling techniques such as GC or evanescent-field coupling, it is easy to align the fiber to the waveguide positions for high butt-coupling efficiency. In addition, it is also possible to couple to several devices simultaneously. Unlike GC or evanescent waveguide coupling, butt-coupling has the benefit of large fiber-to-waveguide alignment tolerance. Compared to GC, it also have a better wavelength insensitivity. For most waveguide couplers which have tapers at the end, the cleaving has to occur exactly in the end of the taper, with a precision of $\pm 10 \mu\text{m}$. As a comparison, in our design the Part I waveguide has a relatively long length ($500 \mu\text{m}$) during the fabrication, and the silicon chip can be cleaved anywhere in Part I of waveguide, within say $\pm 200 \mu\text{m}$.

Following Part I of the waveguide, Part II is an adiabatic waveguide mode-converter which transforms the loosely-confined mode in Part I to the more-confined mode in Part III. The length of Part II is selected to be about $500 \mu\text{m}$ so the mode conversion happens gradually without noticeable loss. Besides, the length of both Part I and Part II are chosen not to be very long, so the propagation loss of Part I and Part II is still small. Considering a length of $300 \mu\text{m}$ for Part I and a length of $500 \mu\text{m}$ for Part II, and a typical propagation loss of $< 2 \text{ dB/cm}$, the overall propagation loss of Part I plus Part II will be $< 0.16 \text{ dB}$, tolerable for most applications. Finally, Part III waveguide is the region where the mode is more confined. Various structures, such as

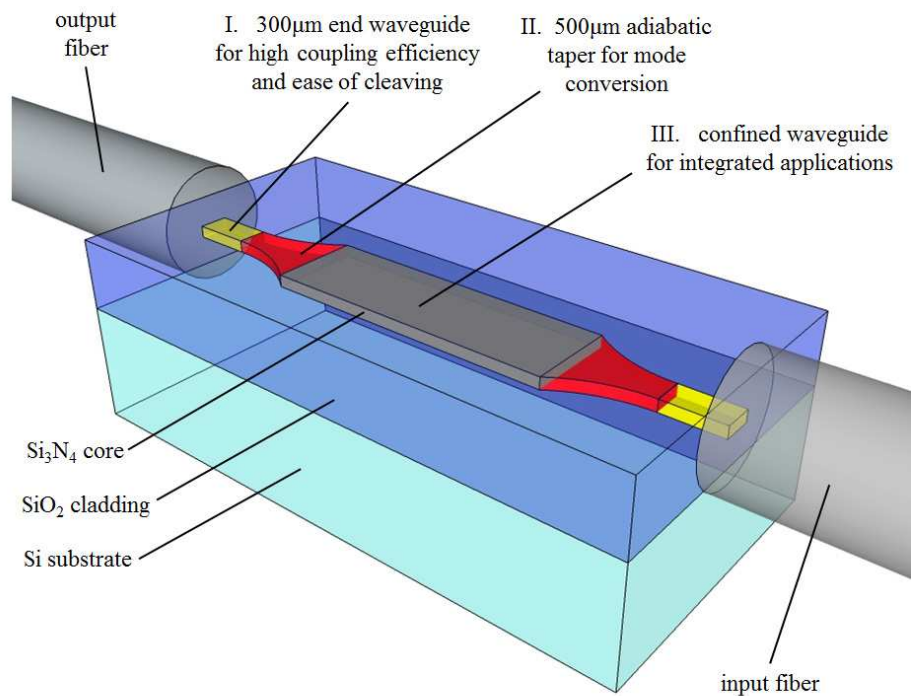


Fig. 1. Diagram of the $\text{Si}_3\text{N}_4/\text{SiO}_2$ waveguide coupler which is composed of three parts. Part I is a straight waveguide with a loosely-confined mode for ultra-broadband high coupling efficiency and insensitivity to cleaving position. Part II is an adiabatic mode-converter which converts the loosely-confined mode to a more-confined mode. Part III is the central areas where the mode is more confined. Depending on future applications, specific structures can be written on Part III. As a proof of demonstration for the coupling efficiency, in this paper Part III is written as a straight waveguide with a more confined mode.

waveguide Bragg gratings (WBG), ring resonators, arrayed waveguide gratings (AWG), etc, can be written and implemented in this region depending on the applications.

For the design and the simulation, an optical simulation software FIMMPROP is used to obtain the mode profiles and calculate the coupling efficiency [19]. The coupling efficiency is calculated by performing the integrals of the field overlap between the fiber mode and the waveguide mode. FIMMPROP also allows the export of a GDSII pattern of the whole waveguide coupler for the experimental fabrication. In order to get a high coupling efficiency, a high numerical aperture (NA) UHNA3 fiber with a small mode size of $4.1 \mu\text{m}$ at the wavelength of 1550 nm is used for the connection with the waveguide coupler. The use of a high NA UHNA3 fiber is not a problem since a low splicing loss of (0.1 dB) with a typical single-mode fibers (i.e. SMF28) can be easily realized [20]. So although in this paper the waveguide coupler is designed to couple with the UHNA3 fiber, our coupler is compatible with a SMF28 fiber provided it is fusion spliced with an UHNA3 fiber.

2.2. Simulation Results

Fig. 2 shows the theoretical coupling efficiency between the UHNA3 fiber and the $\text{Si}_3\text{N}_4/\text{SiO}_2$ waveguide with different waveguide width/thickness geometries. The mode studied here is the fundamental mode of the $\text{Si}_3\text{N}_4/\text{SiO}_2$ waveguide, which is a TE mode with a small mode size, a high effective index and a low propagation loss. The thicknesses of the top and bottom cladding are both $5\ \mu\text{m}$ in the simulations and in the subsequent experiments. A $5\ \mu\text{m}$ top and bottom cladding is thick enough to isolate the mode from being absorbed by the silicon substrate. In the simulation three different Si_3N_4 core thicknesses, 100 nm, 200 nm, and 300 nm, are studied, and for each thickness the coupling efficiency is plotted by varying the Si_3N_4 core width. According to the simulation result, a ultra-high theoretical coupling efficiency of 98 % is obtainable between the UHNA3 fiber and the $\text{Si}_3\text{N}_4/\text{SiO}_2$ waveguide for all three thicknesses of 100 nm, 200 nm and 300 nm, although the maximum coupling efficiency happens at different waveguide widths. Table I lists the maximum theoretical coupling efficiency achievable and the corresponding optimum waveguide geometries. If the Si_3N_4 core thickness is 100 nm, the width of the Si_3N_4 core needs to be about 900 nm to get 98 % coupling efficiency. If the thickness is 200 nm and 300 nm, the optimum Si_3N_4 core width becomes 450 nm and 330 nm, respectively. It is found that the maximum theoretical coupling efficiency is predicted to be a constant value as long as the fiber type and the waveguide core/cladding materials are as stated. In future work, we will present more details on why the maximum theoretical coupling efficiency is a constant value, and we will consider different fibers and different waveguides.

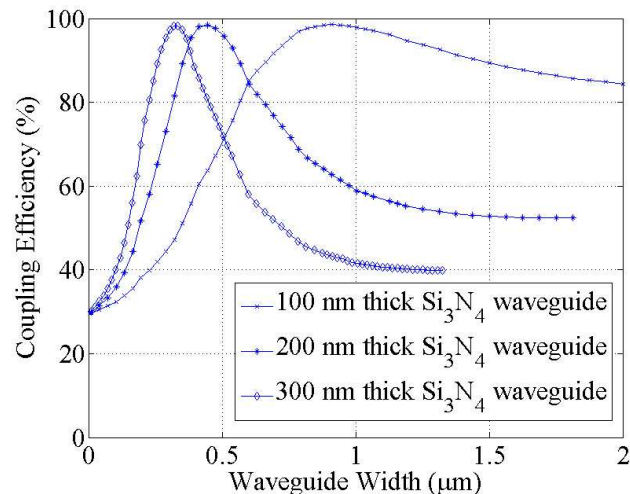


Fig. 2. Theoretical coupling efficiency versus the width of the waveguide between the UHNA3 fiber and the $\text{Si}_3\text{N}_4/\text{SiO}_2$ waveguide for three thickness: 100 nm, 200 nm and 300 nm, at the wavelength of 1550 nm. Although the thickness and the width can vary, the maximum coupling efficiency is predicted to be a constant as long as the fiber type and the waveguide materials are fixed. In this case, the fiber is UHNA3 and the waveguide is $\text{Si}_3\text{N}_4/\text{SiO}_2$, and the maximum theoretical coupling efficiency is 98 %.

To verify the wavelength sensitivity of the coupling efficiency, a plot of the theoretical coupling efficiency as a function of wavelength for these three optimum waveguide geometries, 100 nm \times 900 nm, 200 nm \times 450 nm, and 300 nm \times 330 nm, is given in Fig. 3. As shown before, these three waveguide geometries all give a 98 % theoretical coupling efficiency at the central wavelength of 1550 nm, but their wavelength sensitivities are not the same. The geometry of 100 nm \times 900 nm gives the best wavelength insensitivity, and the coupling efficiency is always higher than 70 % even over a wavelength range of 1 to 2 μm . This is because the mode of 100 nm \times 900 nm Si_3N_4 waveguide is more loosely confined compared to the other two geometries. This

TABLE I
MAXIMUM THEORETICAL COUPLING EFFICIENCIES AT 1550 NM AND THE CORRESPONDING Si_3N_4 THICKNESSES/WIDTHS

Si_3N_4 Thickness	Si_3N_4 Width	Maximum Theoretical Coupling Efficiency
100 nm	900 nm	98.4 %
200 nm	450 nm	98.3 %
300 nm	330 nm	98.4 %

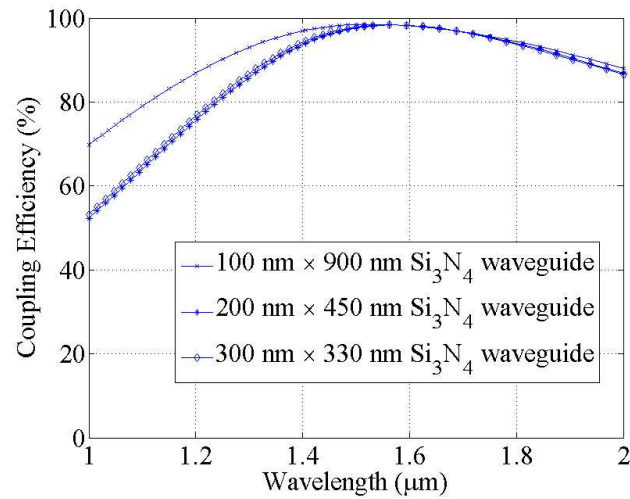


Fig. 3. Theoretical coupling efficiency as a function of wavelength between the UHNA3 fiber and the $\text{Si}_3\text{N}_4/\text{SiO}_2$ waveguide of three optimum geometries in Table I: 100 nm \times 900 nm, 200 nm \times 450 nm, and 300 nm \times 330 nm. These three geometries all give a theoretical coupling efficiencies of 98 % at the wavelength of 1550 nm. The coupling efficiency is least wavelength-sensitive for 100 nm thick, 900 nm wide Si_3N_4 waveguide.

geometry has a high aspect-ratio (width / thickness) waveguide geometry with a low confinement factor. The mode field is mostly out of the core region for the 100 nm \times 900 nm waveguide, and therefore the mode field diameter does not depend sensitively on wavelength. On the other hand, the wavelength sensitivities of the 200 nm \times 450 nm and the 300 nm \times 330 nm waveguides are similar but are not as good as for the 100 nm \times 900 nm waveguide. This is because the mode for the 200 nm \times 450 nm and the 300 nm \times 330 nm geometries are more confined.

Finally, another important feature to consider is the alignment tolerances between the fiber and the waveguide. It is defined as the 3-dB width (FWHM) in a plot of the coupling efficiency versus the displacement in the x- and y- direction. This parameter indicates whether the coupling efficiency will drop substantially or not when the center of the fiber is moved horizontally or vertically with respect to the waveguide coupler. A large alignment tolerance means that even if the position of the fiber changes by a few microns, a good coupling efficiency (< 3 dB change) can still be maintained. Fig. 4 shows the theoretical alignment tolerances between the UHNA3 fiber and the $\text{Si}_3\text{N}_4/\text{SiO}_2$ waveguide. It is found that the theoretical alignment tolerances are almost the same for all the three waveguide geometries, with 3.6 μm in the horizontal direction and 3.5 μm in the vertical direction.

As a proof-of-concept demonstration, we have fabricated and studied the 100 nm \times 900 nm Si_3N_4 waveguide. This waveguide is expected to give a high coupling efficiency over a broad

spectral range (Fig. 3). Moreover, according to Bowers et al. [8], a thinner Si_3N_4 with a high aspect-ratio is expected to give a smaller propagation loss.

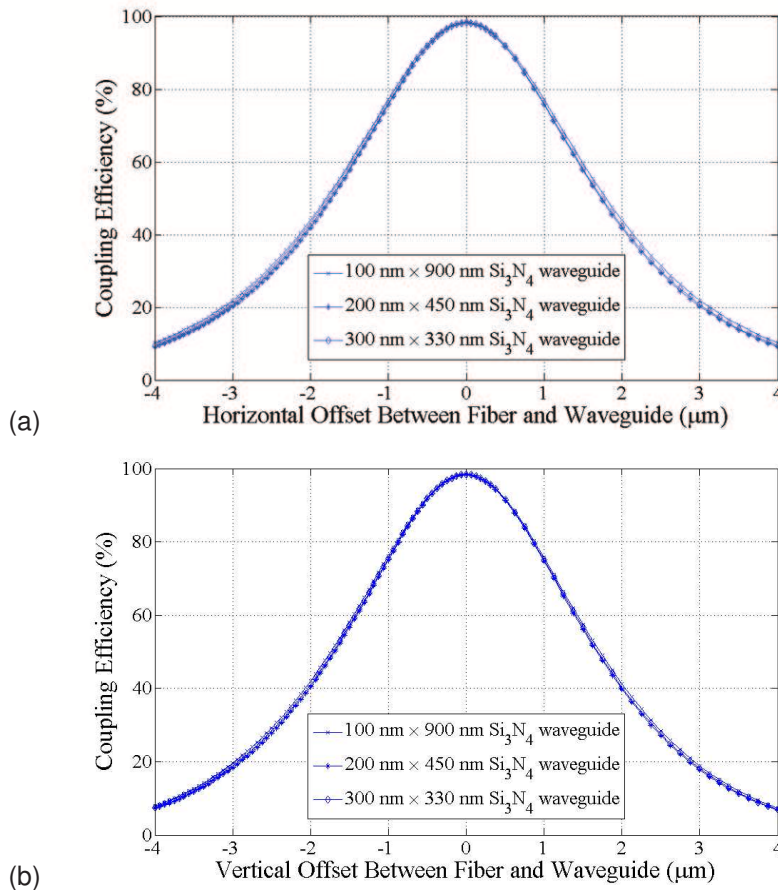


Fig. 4. Theoretical alignment tolerances between the UHNA3 fiber and the $\text{Si}_3\text{N}_4/\text{SiO}_2$ waveguide of three different geometries: 100 nm \times 900 nm, 200 nm \times 450 nm, and 300 nm \times 330 nm. It is defined as the 3-dB width in the plot of the coupling efficiency versus offset. The theoretical alignment tolerances are 3.6 μm horizontally and 3.5 μm vertically for all three waveguide geometries. (a) horizontal alignment tolerance. (b) vertical alignment tolerance.

3. Fabrication and Experimental Results

3.1. Fabrication and Experimental Set-up

The fabrication starts with a silicon wafer with a 5 μm thermal SiO_2 layer on top. A 100 nm thick Si_3N_4 layer is then deposited using low-pressure chemical vapor deposition (LPCVD). The shape of the waveguide coupler is defined by electron-beam (e-beam) lithography. Following this, a 10 nm thick chromium hard mask is deposited by e-beam deposition followed by a lift-off process. Then reactive-ion etching (RIE) is performed and the chromium mask is removed, followed by another 5 μm SiO_2 layer deposited by plasma-enhanced chemical vapor deposition (PECVD) as the upper cladding layer. Finally, the thickness of the whole sample is polished down from the backside from 500 μm originally to about 100 μm , using a lapping jig. The waveguide coupler is then cleaved in the middle of Part I waveguide with a good cleaving position tolerance of ± 200 μm . The whole fabrication process requires only one lithography step and one etching step.

It is noted that there are two extra benefits brought by this waveguide coupler design. First,

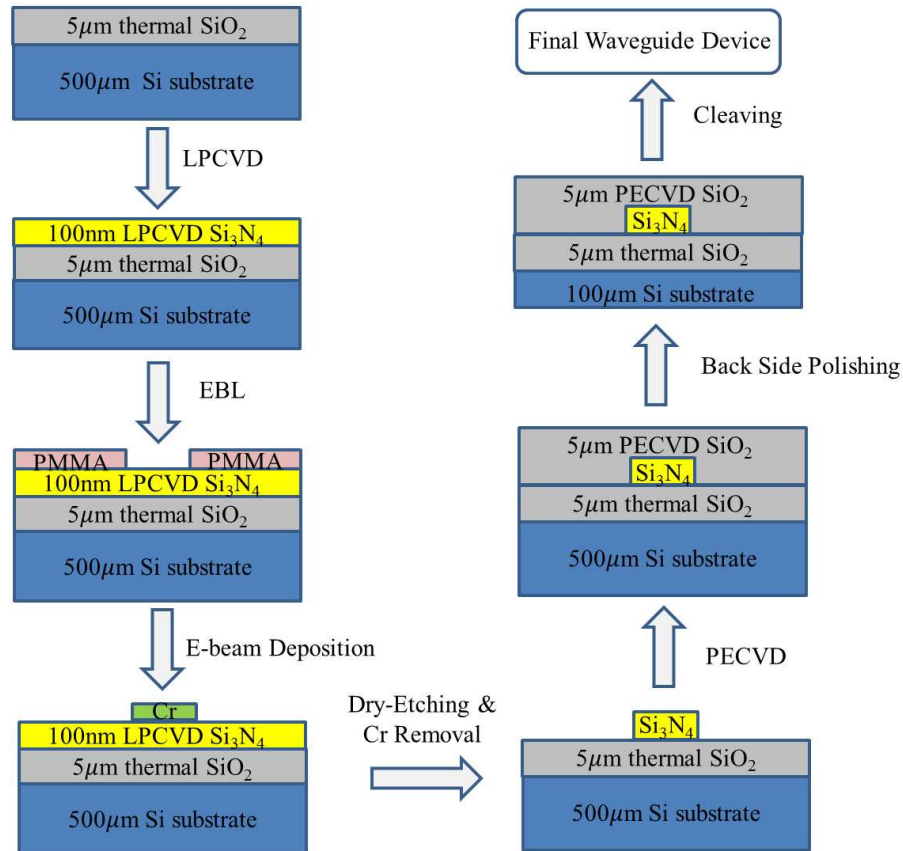


Fig. 5. Fabrication procedures of the Si₃N₄/SiO₂ waveguide coupler with waveguide core thickness of 100 nm. The end-facet cleaving process does not need high position accuracy, thanks to the addition of the Part I waveguide on both sides of the waveguide.

since the width of the Part I high coupling efficiency waveguide is 900 nm, the pattern can be easily done by deep-UV lithography which would lead to higher yield as compared to e-beam lithography. Secondly, since the cleaving tolerance is high, the cleaving can take place almost anywhere in Part I of the waveguide. A direct cleaving process without any back-side polishing is also possible, which will save time and reduce the complexity of the fabrication process. A 500 μm thick waveguide sample is also much more robust than the 100 μm waveguide sample obtained after back-side polishing. In our experiment, we have demonstrated not only cleaving after back-side polishing of a 100 μm thick sample, but also direct cleaving of the sample with a 500 μm thickness.

Fig. 6 shows the experimental set-up for the waveguide performance measurement. The characterization set-up utilizes two XYZ translation stages, each holding a fiber for butt-coupling on both sides of the waveguide coupler. Two measurement methods are used. In the first method, a Superluminescent Diode (SLD) broadband light source (Thorlabs S5FC1550P-A2) is used as the light source, and a 3-paddle fiber polarization controller (PC) is used to control the polarization of the input light to the TE mode. As shown in the previous part, a theoretical coupling efficiency of 98 % is expected at the wavelength of 1550 nm. Similarly, an output fiber is butt-coupled to the other side of the waveguide coupler for maximum power output. Finally, an Optical Spectral Analyzer (OSA) is used to record the transmission spectrum of the waveguide coupler. In the second measurement method, a tunable laser and a power meter are used instead of the SLD broadband light source and the OSA. Both set-ups give the same results for the coupling efficiency.

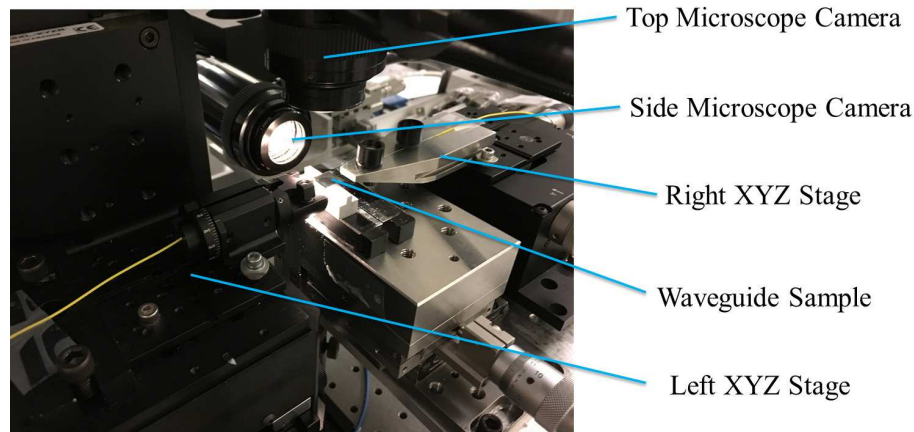


Fig. 6. Experimental set-up for the waveguide performance measurement, showing two XYZ stages which hold input and output fibers, two microscope cameras for fiber/waveguide alignment and a waveguide sample mounted in the middle.

To measure the coupling efficiency of the waveguide coupler, the throughput of two perfectly cleaved and aligned fibers (without the waveguide coupler in the middle) is measured, which represents the reference level for the fiber-to-fiber transmission. Then the $\text{Si}_3\text{N}_4/\text{SiO}_2$ waveguide coupler is positioned between the two fibers, and the light is coupled into and out of the $\text{Si}_3\text{N}_4/\text{SiO}_2$ waveguide coupler by carefully adjusting the input and output fibers for maximum transmission. The difference between the fiber-to-fiber transmission and the fiber-waveguide-fiber transmission includes the coupling losses from both facets plus the propagation loss. To find out the coupling efficiency, waveguide couplers with different lengths of 5 mm, 10 mm, and 15 mm are fabricated and cleaved. The transmission difference allows the extraction of both the propagation loss and the coupling efficiency. An index-matching gel is used to eliminate unwanted reflections.

3.2. Experimental Results

Fig. 7 shows the experimental coupling efficiency as a function of wavelength between the UHNA3 fiber and the 100 nm thick \times 900 nm wide Si_3N_4 waveguide. The wavelength dependence of the coupler is measured from 1450 nm to 1650 nm. The experimental coupling efficiency is 96 % at the central design wavelength of 1550 nm, and is > 90 % for the entire spectral range from 1450 nm to 1650 nm. These results nicely agree with the simulation data. The wobble in the measured coupling efficiency is due to the fact that UHNA3 fiber is not a pure Polarization-Maintaining (PM) fiber, so although the fiber is tuned to a pure TE mode at one wavelength, at other wavelengths there will be some amount of TM mode that will appear. A further discussion about the coupling efficiency versus both TE and TM modes will be given in the next section.

We also obtained the alignment tolerances between the fiber and the waveguide coupler. We first optimized the coupling for maximum transmission and then offset the fiber position both horizontally and vertically. Fig. 8 shows the theoretical and experimental coupling efficiency versus the offset, and Table. II lists the experimental alignment tolerances both in the horizontal and the vertical direction. The experimental alignment tolerances are $3.8 \mu\text{m}$ horizontally and $3.6 \mu\text{m}$ vertically, agreeing well with the theoretical values of $3.6 \mu\text{m}$ and $3.5 \mu\text{m}$ respectively.

4. Further Discussions and Applications

4.1. Coupling Efficiency vs Polarization

In many applications, the waveguide device mainly operates in the fundamental TE mode, which has the highest effective index, the smallest mode size suitable for integration and also the lowest

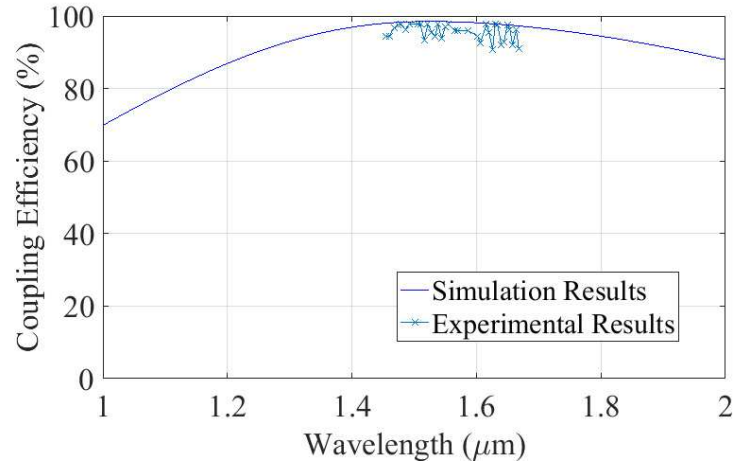


Fig. 7. Theoretical and experimental coupling efficiency as a function of wavelength between the UHNA3 fiber and the 100 nm × 900 nm Si₃N₄ waveguide, which describes how much light is coupled from the UHNA3 fiber to the 100 nm × 900 nm Si₃N₄ waveguide. The experimental coupling efficiency at 1550 nm is 96 %, and is > 90 % for the entire spectrum from 1450 nm to 1650 nm.

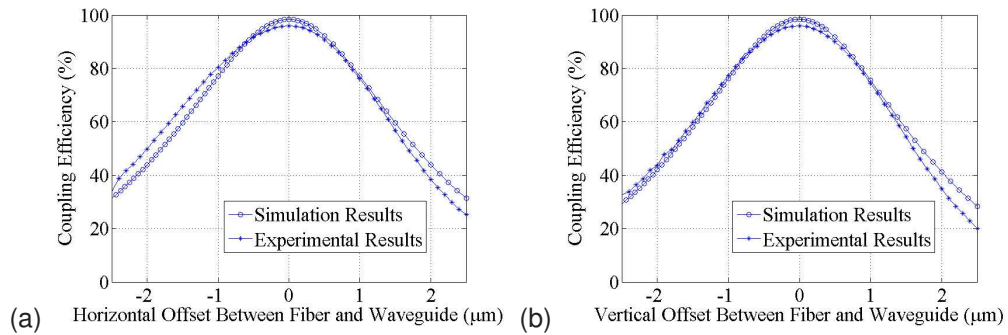


Fig. 8. Theoretical and experimental alignment tolerance between the UHNA3 fiber and the 100 nm × 900 nm Si₃N₄ waveguide. (a) horizontal alignment tolerance. (b) vertical alignment tolerance.

propagation loss. However, sometimes an integrated waveguide device needs to work specifically in the TM mode, or in both the TE and the TM modes. In these cases, a polarization-insensitive coupling efficiency is desired.

Fig. 9 gives the comparison between the TE mode and the TM mode for the theoretical coupling efficiency, for the Si₃N₄/SiO₂ waveguide for the three different geometries: 100 nm × 900 nm, 200 nm × 450 nm, and 300 nm × 330 nm. The difference of the coupling efficiency between the TE mode and the TM mode is obvious for the 100 nm × 900 nm Si₃N₄ waveguide, and their

TABLE II
THEORETICAL AND EXPERIMENTAL ALIGNMENT TOLERANCES BETWEEN THE UHNA3 FIBER AND THE 100 NM × 900 NM Si₃N₄/SiO₂ WAVEGUIDE

	Simulation Data	Experimental Data
Horizontal Direction	3.6 μm	3.8 μm
Vertical Direction	3.5 μm	3.6 μm

performance are very similar for the Si_3N_4 with $300 \text{ nm} \times 330 \text{ nm}$ geometry. The reason for this behavior lies in the aspect-ratio of the waveguide geometry, which is defined as the ratio of the waveguide width divided by the waveguide thickness. Waveguides with aspect-ratios close to unity have square-like cross-sections. It means that the TE mode has a similar mode profile as the TM mode, just with a 90 degree rotational difference. Therefore, a $300 \text{ nm} \times 330 \text{ nm}$ Si_3N_4 waveguide is preferred if polarization insensitivity is the priority, and a $100 \text{ nm} \times 900 \text{ nm}$ Si_3N_4 waveguide is more desirable if wavelength insensitivity is desired for the fundamental TE mode. Table III lists the mode sizes for the three waveguide geometries both horizontally and vertically. We will provide a more detailed study of the polarization-insensitive operation of the waveguide coupler in future work.

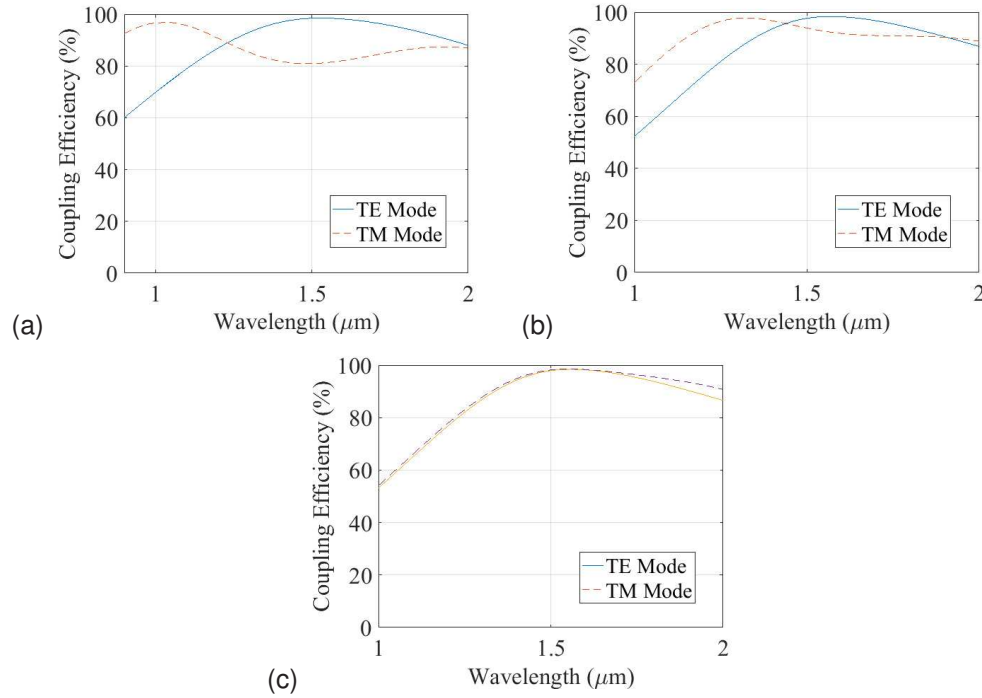


Fig. 9. Theoretical coupling efficiency versus the operating wavelength between the UHNA3 fiber and the $\text{Si}_3\text{N}_4/\text{SiO}_2$ waveguide for both the TE mode and the TM mode. (a) $100 \text{ nm} \times 900 \text{ nm}$ Si_3N_4 waveguide. (b) $200 \text{ nm} \times 450 \text{ nm}$ Si_3N_4 waveguide. (c) $300 \text{ nm} \times 330 \text{ nm}$ Si_3N_4 waveguide.

TABLE III
MODE SIZES ($\frac{1}{e^2}$ INTENSITY WIDTH) OF BOTH TE AND TM MODES FOR THREE $\text{Si}_3\text{N}_4/\text{SiO}_2$ WAVEGUIDE GEOMETRIES

	TE Mode at 1550 nm		TM Mode at 1550 nm	
	horizontal	vertical	horizontal	vertical
$100 \text{ nm} \times 900 \text{ nm}$	$1.89 \mu\text{m}$	$1.67 \mu\text{m}$	$5.71 \mu\text{m}$	$4.55 \mu\text{m}$
$200 \text{ nm} \times 450 \text{ nm}$	$1.56 \mu\text{m}$	$1.46 \mu\text{m}$	$2.75 \mu\text{m}$	$2.71 \mu\text{m}$
$300 \text{ nm} \times 330 \text{ nm}$	$1.71 \mu\text{m}$	$1.66 \mu\text{m}$	$1.66 \mu\text{m}$	$1.70 \mu\text{m}$

4.2. Applications

The waveguide coupler described here exhibits important properties, such as ease of cleaving, high coupling efficiency and ultra-broadband wavelength insensitivity, which make it attractive for a number of applications, including integrated optical filters, WDM systems, quantum information processing, and other optical networks. In one of our recent work, the waveguide coupler with a thickness of 100 nm is used in a Complex Waveguide Bragg Grating (CWBG) as a complex optical filter, which removes as many as 20 randomly-distributed spectral lines in the transmission spectrum [21]. According to the theoretical algorithm, the CWBG has a Si_3N_4 layer with a constant thickness of 100 nm everywhere, and it works on the TE mode for a broad spectrum between 1500 nm and 1550 nm. All these requirements make the 100 nm thick Si_3N_4 waveguide coupler an ideal coupler for the CWBG. In our design, the CWBG utilizes two 100 nm thick Si_3N_4 waveguide on both ends for maximum coupling efficiency, and has aperiodic complex waveguide grating structures written on Part III according to Fig. 1.

Another potential application of the waveguide coupler is for Arrayed Waveguide Gratings (AWG). An AWG is used as an optical (de)multiplexers in wavelength division multiplexed (WDM) systems. Designed to operate over a broad-band spectrum, the input of the AWG is generally an optical fiber containing light of different wavelengths, and at its output the wavelengths are dispersed and come out from different output channels. In a recent paper, an AWG has been realized on the silica-on-silicon platform with 50 nm thick Si_3N_4 waveguide, with the benefit of ultra low propagation loss [22]. The coupling efficiency of the AWG, however, was not optimized fully at 1550 nm. The design and concept of the wavelength-insensitive high coupling efficiency couplers described in this paper could be easily added to the AWGs for better throughput. As a proof of demonstration, we have also successfully combined the same type of the coupler in this paper with a new type of AWGs, which are specifically designed for astronomical observations [23].

5. Conclusions

In this paper, the concept of a fiber-to-waveguide coupler based on a $\text{Si}_3\text{N}_4/\text{SiO}_2$ waveguide is theoretically presented and experimentally analyzed. The waveguide coupler features a high coupling efficiency of 98 % in theory and 96 % in our experiment performed at a wavelength of 1550 nm, and > 90 % experimental coupling efficiency in the spectral range from 1450 nm to 1650 nm. It also features ease of end-facet cleaving position accuracy and large fiber-to-waveguide alignment tolerances both vertically and horizontally. The horizontal and vertical alignment tolerances are 3.8 μm and 3.6 μm experimentally, compared to the theoretical values of 3.6 μm and 3.5 μm respectively. This type of waveguide coupler is particularly useful in applications such as integrated optical filters, WDM systems, quantum information processing, and other optical networks. All the experimental results agrees well with the theoretical values. While this paper focuses on the coupling mechanism implemented using the $\text{Si}_3\text{N}_4/\text{SiO}_2$ waveguide, this good agreement between measured and predicted values suggests that the same concept and approach can be applied to other platforms, material systems, and fiber types. Future work will include a detailed study of the polarization-insensitive waveguide couplers, high coupling efficiency to other types of single-mode fibers, and a scattering loss optimization of the adiabatic mode-converters.

Acknowledgements

The authors wish to thank Prof. Andrew Harris, University of Maryland, for helpful discussions on the coupling mechanism, and also Vincent Brulis for the discussions on FIMMWAVE / FIMMPROP. The authors also thank the W. M. Keck Foundation for financial support of this work.

References

- [1] M. J. Heck, J. F. Bauters, M. L. Davenport, D. T. Spencer, and J. E. Bowers, "Ultra-low loss waveguide platform and its integration with silicon photonics," *Laser & Photonics Reviews*, vol. 8, no. 5, pp. 667–686, 2014.
- [2] D. J. Moss, R. Morandotti, A. L. Gaeta, and M. Lipson, "New cmos-compatible platforms based on silicon nitride and hydrex for nonlinear optics," *Nature Photonics*, vol. 7, no. 8, pp. 597–607, 2013.
- [3] H. Yu, M. Chen, Q. Guo, M. Hoekman, H. Chen, A. Leinse, R. G. Heideman, R. Mateman, S. Yang, and S. Xie, "Si₃N₄-based integrated optical analog signal processor and its application in rf photonic frontend," *Photonics Journal, IEEE*, vol. 7, no. 5, pp. 1–9, 2015.
- [4] L. Zhuang, D. Marpaung, M. Burla, W. Beeker, A. Leinse, and C. Roeloffzen, "Low-loss, high-index-contrast si₃n₄/sio₂ optical waveguides for optical delay lines in microwave photonics signal processing," *Optics express*, vol. 19, no. 23, pp. 23 162–23 170, 2011.
- [5] V. M. Passaro, M. La Notte, B. Troia, L. Passaquindici, F. De Leonardis, and G. Giannoccaro, "Photonic structures based on slot waveguides for nanosensors: State of the art and future developments," *Int. J. Res. Rev. Appl. Sci*, vol. 11, no. 3, pp. 402–418, 2012.
- [6] G. Yurtsever, B. Považay, A. Alex, B. Zabihian, W. Drexler, and R. Baets, "Photonic integrated mach-zehnder interferometer with an on-chip reference arm for optical coherence tomography," *Biomedical optics express*, vol. 5, no. 4, pp. 1050–1061, 2014.
- [7] J. P. Epping, T. Hellwig, M. Hoekman, R. Mateman, A. Leinse, R. G. Heideman, A. van Rees, P. J. van der Slot, C. J. Lee, C. Fallnich *et al.*, "On-chip visible-to-infrared supercontinuum generation with more than 495 thz spectral bandwidth," *Optics express*, vol. 23, no. 15, pp. 19 596–19 604, 2015.
- [8] J. F. Bauters, M. J. Heck, D. John, D. Dai, M.-C. Tien, J. S. Barton, A. Leinse, R. G. Heideman, D. J. Blumenthal, and J. E. Bowers, "Ultra-low-loss high-aspect-ratio Si₃N₄ waveguides," *Optics Express*, vol. 19, no. 4, pp. 3163–3174, 2011.
- [9] J. F. Bauters, M. J. Heck, D. D. John, J. S. Barton, C. M. Bruinink, A. Leinse, R. G. Heideman, D. J. Blumenthal, and J. E. Bowers, "Planar waveguides with less than 0.1 db/m propagation loss fabricated with wafer bonding," *Optics Express*, vol. 19, no. 24, pp. 24 090–24 101, 2011.
- [10] C. R. Doerr, L. Chen, Y.-K. Chen, and L. L. Buhl, "Wide bandwidth silicon nitride grating coupler," *IEEE Photonics Technology Letters*, vol. 22, no. 19, pp. 1461–1463, 2010.
- [11] A. Subramanian, P. Neutens, A. Dhakal, R. Jansen, T. Claes, X. Rottenberg, F. Peyskens, S. Selvaraja, P. Helin, B. Dubois *et al.*, "Low-loss singlemode PECVD silicon nitride photonic wire waveguides for 532–900 nm wavelength window fabricated within a CMOS pilot line," *Photonics Journal, IEEE*, vol. 5, no. 6, pp. 2 202 809–2 202 809, 2013.
- [12] H. Zhang, C. Li, X. Tu, J. Song, H. Zhou, X. Luo, Y. Huang, M. Yu, and G. Lo, "Efficient silicon nitride grating coupler with distributed Bragg reflectors," *Optics Express*, vol. 22, no. 18, pp. 21 800–21 805, 2014.
- [13] W. D. Sacher, Y. Huang, L. Ding, B. J. Taylor, H. Jayatileka, G.-Q. Lo, and J. K. Poon, "Wide bandwidth and high coupling efficiency Si₃N₄-on-SOI dual-level grating coupler," *Optics Express*, vol. 22, no. 9, pp. 10 938–10 947, 2014.
- [14] S. Tao, J. Song, Q. Fang, M. Yu, G. Lo, and D. Kwong, "Improving coupling efficiency of fiber-waveguide coupling with a double-tip coupler," *Optics Express*, vol. 16, no. 25, pp. 20 803–20 808, 2008.
- [15] L. Chen, C. R. Doerr, Y.-K. Chen, and T.-Y. Liow, "Low-Loss and Broadband Cantilever Couplers Between Standard Cleaved Fibers and High-Index-Contrast Si N or Si Waveguides," *Photonics Technology Letters, IEEE*, vol. 22, no. 23, pp. 1744–1746, 2010.
- [16] T. Tiecke, K. Nayak, J. Thompson, T. Peyronel, N. De Leon, V. Vuletić, and M. Lukin, "Efficient fiber-optical interface for nanophotonic devices," *Optica*, vol. 2, no. 2, pp. 70–75, 2015.
- [17] P. Rousselot, C. Lidman, J.-G. Cuby, G. Moreels, and G. Monnet, "Night-sky spectral atlas of OH emission lines in the near-infrared," *Astronomy and Astrophysics*, vol. 354, pp. 1134–1150, 2000.
- [18] J. Bland-Hawthorn, A. Buryak, and K. Kolossovski, "Optimization algorithm for ultrabroadband multichannel aperiodic fiber Bragg grating filters," *JOSA A*, vol. 25, no. 1, pp. 153–158, 2008.
- [19] "Fimmwave/fimmprop," *Photon Design Ltd*. <http://www.photond.com>.
- [20] "Application note nuapp-3: Uhna fiber efficient coupling to silicon waveguides," *Nufern Inc* http://www.nufern.com/pam/optical_fibers/984/UHNA3/.
- [21] T. Zhu, Y. Hu, P. Gatkine, S. Veilleux, J. Bland-Hawthorn, and M. Dagenais, "Arbitrary on-chip optical filter using complex waveguide bragg gratings," *Applied Physics Letters*, vol. 108, no. 10, p. 101104, 2016.
- [22] D. Dai, Z. Wang, J. F. Bauters, M.-C. Tien, M. J. Heck, D. J. Blumenthal, and J. E. Bowers, "Low-loss Si₃N₄ arrayed-waveguide grating (de) multiplexer using nano-core optical waveguides," *Optics Express*, vol. 19, no. 15, pp. 14 130–14 136, 2011.
- [23] P. Gatkine, S. Veilleux, Y. Hu, T. Zhu, Y. Meng, J. Bland-Hawthorn, and M. Dagenais, "Development of high resolution arrayed waveguide grating spectrometers for astronomical applications: first results," *preprint (arXiv: 1606.02730)*, 2016.